

Contents lists available at ScienceDirect

Petroleum Science

journal homepage: www.keaipublishing.com/en/journals/petroleum-science



Original Paper

A comprehensive fracture characterization method for shale reservoirs



Chen Zhang ^{a, b, c, d}, Zong-Quan Hu ^{a, b, *}, Xiang-Ye Kong ^{c, **}, Bo Gao ^{a, b}, Jia-Yi Liu ^{a, b}, Yu-Han Huang ^{c, d}, Hua-Dong Chen ^{c, d}

- ^a State Key Laboratory of Shale Oil and Gas Enrichment Mechanisms and Effective Development, Beijing, 100083, China
- ^b SINOPEC Key Laboratory of Shale Oil/Gas Exploration and Production Technology, Beijing, 100083, China
- ^c State Key Laboratory of Oil and Gas Reservoir Geology and Exploitation, Chengdu University of Technology, Chengdu, 610059, Sichuan, China
- d Institute of Sedimentary Geology, Chengdu University of Technology, Chengdu, 610059, Sichuan, China

ARTICLE INFO

Article history: Received 7 February 2024 Received in revised form 14 January 2025 Accepted 18 March 2025 Available online 21 March 2025

Edited by Jie Hao

Keywords: Shale reservoir Fracture characterization Logging analysis Reservoir evaluation Lucaogou formation

ABSTRACT

Opening-mode fractures play a crucial role in shale reservoirs, as they serve as flow channels and provide storage space for hydrocarbons. The shale reservoirs in the Permian Lucaogou Formation of the Junggar Basin, NW China, record multi-stage tectonic and diagenetic processes that created multi-stage natural fractures, thereby contributing to the oil content differentiation within the formation. Effective identification and characterization of natural fractures is vital for the efficient recovery of shale oil in the Jimsar Sag. We combine outcrop observations, drill core analyses, thin section examinations, and well log analyses to determine the characteristics of fractures in the shale reservoirs and their modes of development. We also establish multi-parameter evaluation index criteria and an evaluation system for fractures using statistical analyses. The shale reservoirs of the Lucaogou Formation in the Jimsar Sag host three main types of fracture: tectonic fractures, diagenetic fractures, and overpressure fractures. Conventional well logging, imaging logging, and core observations demonstrate that the fractured shale reservoir section has gamma-ray counts (GR) of >75 API, shallow laterolog resistivities of <80 $\Omega \cdot m$, neutron densities of $<2.40 \text{ g/cm}^3$, neutron porosities of >27%, and interval transit times of $>23.77 \mu\text{s/m}$, fracture density exceeding 3 fractures/m, and average porosity ranging from 0.2% to 0.3% in the lower sweet spots. The lower sweet spot (P₂I₁²) of the Lucaogou Formation exhibits the highest degree of fracture development. Our detailed characterization reveals high fracture permeabilities and porosities in the upper and lower sweet spots $(P_2|_2^2)$ and $(P_2|_2^2)$, with higher values in the latter. In addition, we present a novel rose diagram method to represent various fracture parameters. The best-developed tectonic fractures in the Lucaogou Formation strike ENE-WSW, have an average linear density of 1.65 fractures/m, an average aperture of 0.25 mm, an average length of 8.7 cm, and the highest proportion of unfilled fractures. Our study shows that a combination of field observations, drill core analyses, microscopic observations, and well logging provides a solid foundation for investigating the mechanisms of fracture formation in shale

© 2025 The Authors. Publishing services by Elsevier B.V. on behalf of KeAi Communications Co. Ltd. This is an open access article under the CC BY-NC-ND license (http://creativecommons.org/licenses/by-nc-nd/4.0/).

1. Introduction

Global interest in unconventional oil and gas resources has surged in the 21st century. Despite substantial advancements in

E-mail addresses: zongquanhu1979@163.com (Z.-Q. Hu), kongxiangyecup@163.com (X.-Y. Kong).

shale oil and gas research, significant gaps persist in understanding certain geological and exploration facets (Curtis, 2002; Fu et al., 2020; Jia et al., 2012; Zou et al., 2010, 2012; Zhang et al., 2023). Many of the fundamental theories, controlling factors, evaluation criteria, and exploration strategies that are required to assess the resource potential of shale oil deposits remain unresolved (Qiu et al., 2012; Feng et al., 2021; Zou et al., 2012, 2015). Unlike the natural gas that accumulates in conventional reservoirs, shale gas occurs in shale/mudstone formations in three forms: free gas,

^{*} Corresponding author.

^{**} Corresponding author.

C. Zhang, Z.-Q. Hu, X.-Y. Kong et al.

Petroleum Science 22 (2025) 2660–2676

adsorbed gas, and dissolved gas (Curtis, 2002; Zou et al., 2010). Therefore, pore structure is a key factor in shale gas enrichment, and opening-mode fractures play a vital role, as they influence the gas content and occurrence of shale gas (Jia et al., 2012; Zou et al., 2012; Yang et al., 2013; Wang et al., 2017; Xu et al., 2019; Zheng et al., 2019). Accordingly, investigation of the fractures in shale is essential in any assessment of shale oil and gas resources, and it has become a prominent area of research in petroleum geology for unconventional hydrocarbons (Zhang et al., 2024) (see Tables 1–4).

Shale reservoirs, comprising fine-grained sedimentary rocks with low matrix permeability (Thomas and Ward, 1972; Nelson, 2009; Ghanizadeh et al., 2015), primarily rely on natural fractures as dominant flow channels for hydrocarbon emplacement. Understanding natural fractures is crucial for pinpointing sweet spots in shale oil and gas reservoirs, minimizing drilling and completion costs (Olson et al., 2009; Fall et al., 2012; Fall et al., 2015; Laubach et al., 2016, 2019). Previous studies have employed multi-scale characterization and multi-factor analyses utilizing core and thinsection observations to scrutinize fractures in mudstone/shale (Chalmers et al., 2012; Gale et al., 2014; Clarkson et al., 2013; Tian et al., 2013; Lu et al., 2016; Slatt and O'Brien, 2011; Zhang et al., 2017; Zhang et al., 2017; Laubach et al., 2019). However, mudstone/shale rich in organic matter fosters extensive micro-to nano-pores with complex structures influenced by multiple factors (Tang et al., 2016; Liu et al., 2017; Zan et al., 2017).

Since the Paleozoic, multiple tectonic movements have modified the geological features of the Jimsar Sag. These tectonic events occurred during the late Paleozoic, Mesozoic, and Cenozoic, resulting in a complex stratigraphic configuration and distinctive structural characteristics. Consequently, the Jimsar Sag possesses abundant opening-mode fractures. Furthermore, the complex processes of diagenesis and hydrocarbon generation and expulsion within the sag have heavily influenced fracture apertures. Such natural fractures were a critical factor in the differentiation of oil contents within shale reservoirs of the Jimsar Sag. Previous studies on shale oil in the Jimsar Sag have focused mainly on the regional structure (Yang et al., 2012; Zheng et al., 2018), reservoir rock lithology (Cao et al., 2019), pore structure (Liu et al., 2019; Tian et al., 2019), and sedimentary characteristics (Zhang et al., 2018; Ma et al., 2019). However, the investigation and characterization of natural fractures have received less attention, thereby restricting the efficient development of shale oil.

Our research employed a range of methodologies to identify fractures accurately within the shale oil reservoirs of the Permian Lucaogou Formation in the Jimsar Sag. Our study aimed to clarify the types of fracture and their characteristics, and to establish comprehensive parameters for fracture characterization and an evaluation system specifically tailored for shale oil reservoirs.

2. Geological setting

Located in the southern part of the Central Asian Orogenic Belt (Fig. 1(a)), the Junggar Basin covers an area of $\sim 1.3 \times 10^5$ km². This Mesozoic—Cenozoic sedimentary basin was developed above a Paleozoic basement (Li et al., 2016; Zhang et al., 2017). The Jimsar Sag is in the southeastern part of the Junggar Basin (Fig. 1(b)) and forms a half-graben on the folded middle-Carboniferous basement. The sag is delineated and intersected by a number of faults: e.g., the Jimsar Fault to the north, which separates the sag from the Shaqi Uplift; the Well J1 South No. 1 and Xidi Faults to the west, which separate the sag from the Beisantai Uplift; and the Santai Fault to the south. The elevation of the sag increases to the east, where it transitions into the Guxi Uplift (Fig. 1(c)).

The Jimsar Sag contains rocks of Carboniferous, Permian, Triassic, Jurassic, Cretaceous, Paleogene, Neogene, and Quaternary age. The Permian strata are divided into the Jiangjunmiao, Lucaogou, and Wutonggou formations. With an average thickness of 260 m, the Lucaogou Formation displays continuous hydrocarbon shows and vertically distributed intervals with favorable physical properties and high oil contents, thereby indicating sweet spots. Two sweet spots have been identified in the Lucaogou Formation: an upper sweet spot in the 2nd sand group of the second member of the Lucaogou Formation ($P_2l_2^2$), and a lower sweet spot in the 2nd sand group of the first member ($P_2l_1^2$).

As stated above, the Jimsar Sag has recorded multiple episodes of tectonic movement since the Paleozoic (Zhang et al., 2017, 2025). The Jimsar Fault formed in response to the development of the Shaqi Uplift to the north of the Jimsar Sag during the late Carboniferous. During the early middle Permian, intensive tectonic subsidence occurred within the Jimsar Sag and the Jingjingzigou Formation was deposited. The interior of the limsar Sag was in a lacustrine environment during deposition of the main source rocks of the Lucaogou Formation in the middle Permian. From the late Permian to the Early Triassic, the development of the Beisantai Uplift to the west of the Jimsar Sag was relatively subdued, and the sag was submerged within the sedimentary water column. The sag formed a half-graben during this period of lacustrine deposition. During the Late Triassic, the Shaqi Uplift formed to the east of the Jimsar Sag, leading to extensive denudation of the Triassic and Permian strata in the eastern part of the sag. Continued development of the Shaqi Uplift to the north of the Jimsar Sag caused movement along the Jimsar Fault, leading to intense erosion of the Jurassic strata within the sag (Wu et al., 2015; Qiu et al., 2016; Zhang et al., 2017: Ma et al., 2018).

The Permian Lucaogou Formation in the Junggar Basin is a major target for shale oil. Breakthroughs have been made in shale oil exploration in the eastern Junggar Basin, and industrial oil streams have been obtained from multiple wells in the Lucaogou Formation of the Jimsar Sag, such as wells J30, J174, and J521 (Kong et al., 2021; Kuang et al., 2012; Du et al., 2014). The Jimsar Sag contains high-quality source rocks, with TOC (total organic carbon) commonly above 2%. The organic matter is predominantly Type II1, and the vitrinite reflectance is generally $0.8-1.0\ R_0\%$, corresponding to low maturity to maturity. The oil generation potential of the source rocks is high. The Lucaogou Formation of the Jimsar Sag contains estimated shale oil resources of 0.38 billion tons, demonstrating its huge exploration potential (Kuang et al., 2012; Du et al., 2014; Zhe et al., 2016).

3. Identification and distribution of fractures

3.1. Fracture types

The shale reservoir in the Permian Lucaogou Formation of the Jimsar Sag exhibits well-developed natural fractures, as observed in field outcrops and core samples and by microscopic examination of thin sections. These fractures can be classified into three primary types: structural, diagenetic, and abnormal high-pressure fractures.

Tectonic fractures, notably shear and tensile fractures, are prominent in field outcrops. Conjugate shear fractures, which often form X-shaped patterns (Fig. 2(a) and (b)), are common, and they are long and straight with smooth surfaces featuring slickensides. In cores, shear fractures are often developed as a single branch, with suppressed branching likely due to rock heterogeneities (Fig. 2(d)). Tensile fractures are less common, and they are relatively short and coarse with jagged surfaces. Field outcrop observations indicate that the tensile fractures are typically 1–2 cm long with relatively large apertures of 0.02–0.3 cm (Fig. 2(c)). Core observations show that the tensile fractures are typically filled with quartz and calcite, but locally with argillaceous fillings (Fig. 2(e)).

Table 1Parameter statisties of main conventional well logs of 42 non-fractured sections.

Non-fractured sections	DEN, g⋅cm ⁻³	AC, μm/m	CNL, %	RLLS, Ω·m	GR, API	CAL, cm	SP, mV
J22 (limestone)	2.576	20.17	24.73	262.94	53.9	8.716	-25.85
J22 (mudstone)	2.412	22.96	31.7	115.16	61.88	8.607	-14.87
J22 (siltstone)	2.521	19.58	19.4	243	51.79	8.449	-17.23
J22 (siltstone)	2.545	20.68	21.13	234.5	51.76	8.523	-37.59
J25 (mudstone)	2.574	19.96	19.8	219	51.53	8.716	-15.23
J25 (limestone)	2.591	20.59	18.9	147.7	44.85	8.617	-16.77
J25 (siltstone)	2.339	24.04	29.16	107.39	87.76	8.538	-22.83
J25 (limestone)	2.477	23.09	21.5	139	66.7	8.746	-37.87
J25 (mudstone)	2.503	21.10	21.98	261	49.39	8.483	-14.23
J27 (limestone)	2.524	20.78	20.26	143.6	67.8	8.479	-11.17
J27 (siltstone)	2.521	17.53	16.5	124	51	8.516	-27.65
J27 (mudstone)	2.448	21.56	26.83	146.4	62.56	8.61	-16.87
J27 (siltstone)	2.475	19.85	193	127	54	8.86	-16.54
J173 (limestone)	2.511	23.29	21.7	146	52.7	8.586	-14.37
J173 (mudstone)	2.413	22.82	26.05	101.9	82.9	8.5	-27.08
[173 (siltstone)	2.56	19.82	22.17	110.1	57.2	8.623	-31.44
J36 (mudstone)	2.57	19.85	18.5	127	57.7	8.54	-15.07
[36 (limestone)	2.55	18.72	18.3	173	49.8	8.723	-27.05
J36 (siltstone)	2.51	20.38	21	200	57.1	8.453	-15.62
[37 (mudstone)	2.49	23.43	26.59	124.44	63.61	8.7	-26.07
J37 (mudstone)	2.51	21.09	24.76	180.72	70.68	8.68	-27.01
J37 (siltstone)	2.52	24.68	23.92	172.34	62.3	8.76	-20.62
[37 (limestone)	2.506			173.66		8.586	
[37 (limestone)	2.403			94.24		8.621	
I174 (mudstone)	2.41			147		8.641	
J174 (mudstone)	2.55			160.18		8.46	
[174 (siltstone)	2.56			140.69		8.732	
[31 (marlstone)	2.577			146	50.4	8.858	-28.7
J31 (mudstone)	2.57	23.43	22.3	175	50.7	8.46	-27.05
J31 (mudstone)	2.59	24.13	23.4	147	51.1	8.586	-21.47
[30 (siltstone)	2.54	23.16	25.4	147	57.7	8.76	-21.47
[30 (mudstone)	2.51	19.81	22.4	176	52.7	8.586	-35.71
J30 (limestone)	2.41	23.85	23.59	185	69.46	8.563	-5
J30 (siltstone)	2.45	22.67	25.36	175	62.34	8.64	-35.5
[30 (mudstone)	2.47	23.68	27.35	143	76	8.365	-26.5
I172 (mudstone)	2.48	21.87	24.68	156	70.46	8.325	-40.5
J172 (mudstone)	2.39	21.15	22.34	125	79.40	8.349	-10.5
[172 (siltstone)	2.43	24.55	19.53	125	74.36	8.125	-15.3
J29 (mudstone)	2.45	24.24	18.46	200	71.34	8.496	-19.3 -19.3
J29 (mudstone)	2.44	24.85	20.35	140	68.34	8.756	-19.3 -20.3
J29 (siltstone)	2.41	24.52	21.35	94	66.16	8.459	-20.5 -23.5
J29 (mudstone)	2.45	24.32	26.32	167	67.34	8.354	-23.3 -9.35

Most tensile fractures intersect low-angle shear fractures at high angles (Fig. 2(f)). This indicates that tectonic fractures of different types form a network, potentially serving as channels for hydrocarbon migration.

Diagenetic fractures, primarily bedding fractures, measure 5–15 m in field outcrops, although their apertures are relatively limited, measuring 0.05 cm to 0.1 m (Fig. 2(g)). These fractures are commonly observed in core samples, often penetrating the cores (Fig. 2(h) and (i)).

Abnormal high-pressure fractures are also observed in the cores, and they formed mainly by hydraulic action (Liu et al., 2017; Zhang et al., 2017). Although abnormal high-pressure fractures are observed in the core samples (Fig. 2(j) and (k)) and thin sections (Fig. 2(l)), they are notably absent from field outcrops. Core observations indicate that the fractures are mainly mineral-filled and have low oil contents.

3.2. Fracture identification based on well logs

3.2.1. Fracture identification based on conventional well logs

Well logs, each serving distinct functions, vary in their sensitivity to fractures. Fracture identification in well logs primarily depends on interpretations of lithology, resistivity, and porosity.

Lithology-targeting logs include the caliper (CAL), spontaneous potential (SP), and natural gamma-ray (GR) logs. The SP log highlights sandstone-mudstone interfaces, aiding in lithological boundary identification. The GR log is crucial for assessing permeability, with mudstone, being more radioactive than sandstone and carbonate rocks, distinguishable by its higher gamma-ray readings. Uranium, precipitated along fractures, increases GR values, making it useful for identifying fractured and mudstone sections (Dong et al., 2013). The CAL log detects lithologies by measuring wellbore diameters, which fluctuate due to borehole collapse in fractured zones.

Resistivity-targeting logs, such as dual laterolog and microlog, provide further insights. The dual laterolog, using a guard electrode, reduces mud interference, enhancing vertical resolution. Fractures influence readings, with deep and shallow laterologs (RLLD and RLLS) showing distinct "negative" or "positive" differences based on fracture angles (Zeng et al., 2010). In the Lucaogou Formation, characterized by thin beds and high resistivity, combining dual laterolog with microlog enhances fracture prediction.

Porosity-targeting logs, including the compensated neutron (CNL), density (DEN), and sonic (AC) logs, reveal formation porosity. In argillaceous sections, corrections are necessary (Hong, 1998). The AC log, by analyzing P-wave transit times, identifies fractures filled with fluids or cement, evident through distinct cycle skips.

Table 2 Parameter statisties of main conventional well logs of 41 fractured sections.

Fractured	DEN, g∙cm ⁻³	AC, μm/m	CNL, %	RLLS,	GR, API	CAL, cm	SP, mV
sections				Ω·m			
J31 (siltstone)	2.285			62.19		8.883	
J31 (siltstone)	2.282			40.11		8.751	
J31 (mudstone)	2.297			45.7		8.754	
J31 (mudstone)	2.293			58.39		9.22	
J32 (mudstone)	2.21			32.47		9.154	
J32 (siltstone)	2.34			55.87		9.764	
J32 (siltstone)	2.355	26.05	29.41	48.86	79.61	8.57	-5.41
J32 (mudstone)	2.353	24.84	28.14	36.82	85.46	8.44	-8.53
J32 (siltstone)	2.37	24.86	28.71	47.53	75.44	8.73	-8.43
J34 (siltstone)	2.163	26.79	31.58	40.92	94.23	8.75	-16.97
[34 (siltstone)	2.185	26.4	31.38	25.53	99.46	9.12	-19.21
[34 (mudstone)	2.411	26.05	30.02	69.11	78.19	8.71	-19.15
[36 (marlstone)	2.313	25.01	30.46	38.23	85.64	8.61	-19.5
[36 (mudstone)	2.276	24.96	30.08	34.44	95.16	8.61	-29.54
[36 (fine sandstone)	2.314	25.52	28.52	32.04	88.46	8.81	-27.9
J36 (mudstone)	2.272	29.78	36.85	35.76	85.42	8.64	-27.76
J37 (siltstone)	2.392	24.65	31.65	54.24	81.59	8.36	-26.82
J37 (limestone)	2.268	24.49	30.39	35.26	92.23	8.62	-25.83
J37 (limestone)	2.405	24.08	28.78	57.39	76.23	8.96	-42.22
J37 (limestone)	2.307	23.73	27.37	54.71	80.19	8.78	-42.84
J37 (mudstone)	2.215	33.67	38.89	5.01	89.35	9.34	-19.81
J37 (siltstone)	2.243	34.77	35.4	7.57	97.46	9.11	-18.75
[37 (mudstone)	2.247	30.4	37.48	10.45	87.75	9.01	-18.78
J29 (mudstone)	2.222	25.35	32.71	37.89	94.45	8.67	-36.02
J29 (mudstone)	2.247	25.51	31.75	43.47	91.74	8.73	-37.44
J29 (siltstone)	2.357	29.7	39.75	64.75	81.64	8.46	-27.12
J29 (mudstone)	2.296	29.4	38.21	43.51	85.36	8.64	-23.39
J29 (siltstone)	2.276	27.62	32.56	65.66	97.77	8.73	-14.97
J172 (mudstone)	2.295	24.04	29.51	33.14	94.57	9.04	-10.79
J172 (siltstone)	2.357	24.24	34.5	40.55	81.57	8.76	-12.13
J172 (siltstone)	2.382	27.8	34.63	48.31	81.89	8.68	-17.13
[172 (siltstone)	2.349	29.1	40.59	60.59	83.46	9.03	-16.35
J174 (mudstone)	2.236	29.1	41.52	50.48	95.16	8.32	-10.36
[174 (siltstone)	2.235	30.01	40.35	35.34	88.31	8.98	-26.59
[174 (limestone)	2.258	27.27	39.25	51.35	45.51	8.35	-29.35
J174 (mudstone)	2.263	28.16	38.74	54.36	89.31	8.346	-41.35
J30 (siltstone)	2.159	27.85	36.54	35.36	97.26	8.12	-26.85
J30 (mudstone)	2.236	30.31	36.95	45.84	90.64	8.268	-30.68
J30 (limestone)	2.356	27.57	36.05	70.24	87	8.459	-34.36
J30 (siltstone)	2.289	30.34	38.59	45.25	88	8.354	-2.35
[30 (mudstone)	2.157	29.07	39.99	32.35	99.54	8.321	-2.35 -7.26
Joo (muastone)	2.137	23.07	בב.בכ	32.33	33.34	0,321	-7.20

Table 3Characteristics of the conventional well logs of fractured sections.

	DEN, g⋅cm ⁻³	CNL, %	AC, μm/m	GR, API	RLLS, Ω·m
Fractured section	<2.40	>27	>23.77	>75	<80
Non-fractured section	>2.40	<27	<23.77	<75	>80

Core examination identified 42 non-fractured and 41 fractured sections for analyzing conventional well logs (Fig. 3, Tables 1–2). Seven logs proved effective for fracture characterization, with the GR, AC, CNL, RLLS, and DEN logs showing higher values in fractured sections, indicating increased porosity and fluid presence. The SP and CAL logs, however, showed minimal response to fractures due to the lithological complexity of the Lucaogou Formation.

Key parameters for fracture characterization.

Key elements	Key characterization parameters
Occurrence Scale Filling	Striking direction and dip direction and angle Length and aperture Filling types and filling degrees
Development degrees	Linear density

In summary, fractured sections are characterized by gamma-ray counts >75 API, shallow resistivity <80 Ω ·m, neutron densities <2.40 g/cm³, neutron porosities >27%, and interval transit times >23.77 μ s/m (Table 3).

3.2.2. Fracture identification based on image logs

Borehole imaging techniques provide a detailed depiction of subsurface formations through color-difference processing of microresistivity variations along borehole walls (Wang et al., 2015). Utilizing formation microimager (FMI) technology, resistivity disparities manifest as distinct colors, with lower resistivity regions appearing darker and higher resistivity regions appearing brighter. This color contrast facilitates the differentiation of lithological components, with sandstone typically exhibiting brighter tones and mudstone darker hues. Fractures within FMI images are depicted as planar features intersecting the cylindrical borehole, often forming sinusoidal curves indicative of their trajectory. Analysis of these curves allows for the extraction of critical fracture parameters, including morphology, strike direction, dip direction, and angle, as well as quantification of fracture occurrence, density, and aperture. Notably, fractures containing mud display darker hues due to their lower resistivity, enabling the delineation of fracture development characteristics through imaging logging techniques (Liu et al., 2019). The application of imaging logging

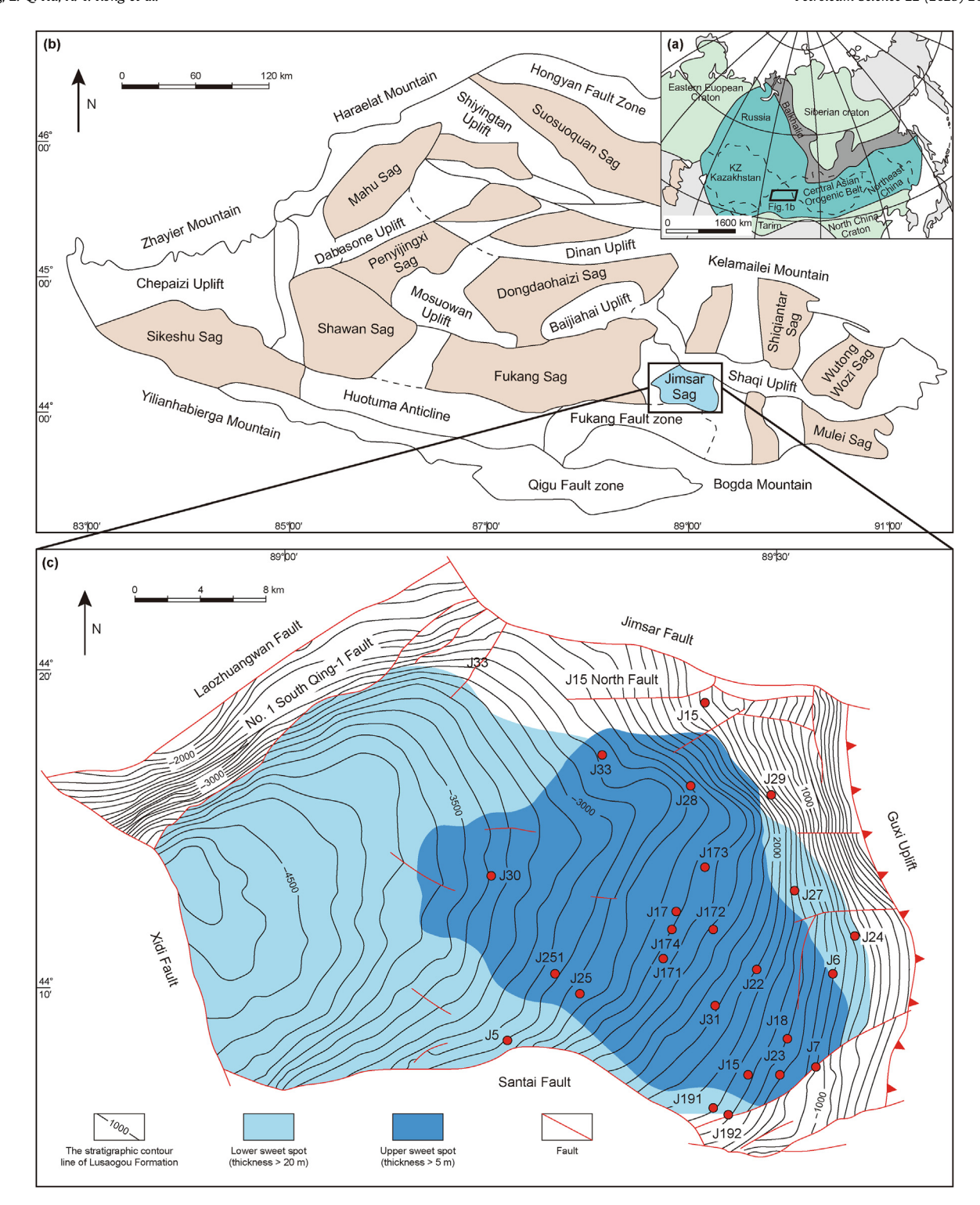


Fig. 1. (a) Geological map of the Central Asian Orogenic Belt (modified after Zhang et al., 2017, 2022). (b) Tectonic units of the Junggar Basin and location of the Jimsar Sag (modified after Li et al., 2016, Zhang et al., 2017, 2022). (c) Tectonic map of the Jimsar Sag (modified after Ma et al., 2018, Liu et al., 2020; Zhang et al., 2022).

facilitates the comprehensive identification of geological attributes, encompassing sedimentary and structural features, each uniquely discernible within FMI images. Notably, FMI images capturing various fracture types within the shale reservoirs of the Permian Lucaogou Formation exhibit distinctive characteristics (Fig. 4), thereby offering a precise means for the accurate identification and

characterization of fractures, thus augmenting our holistic comprehension of the reservoir environment.

In resistivity imaging logging, fracture apertures can be characterized on the basis of the resistivity of fracture fillings. The primary fracture types of the Permian Lucaogou Formation are as follow:

C. Zhang, Z.-Q. Hu, X.-Y. Kong et al.

Petroleum Science 22 (2025) 2660–2676

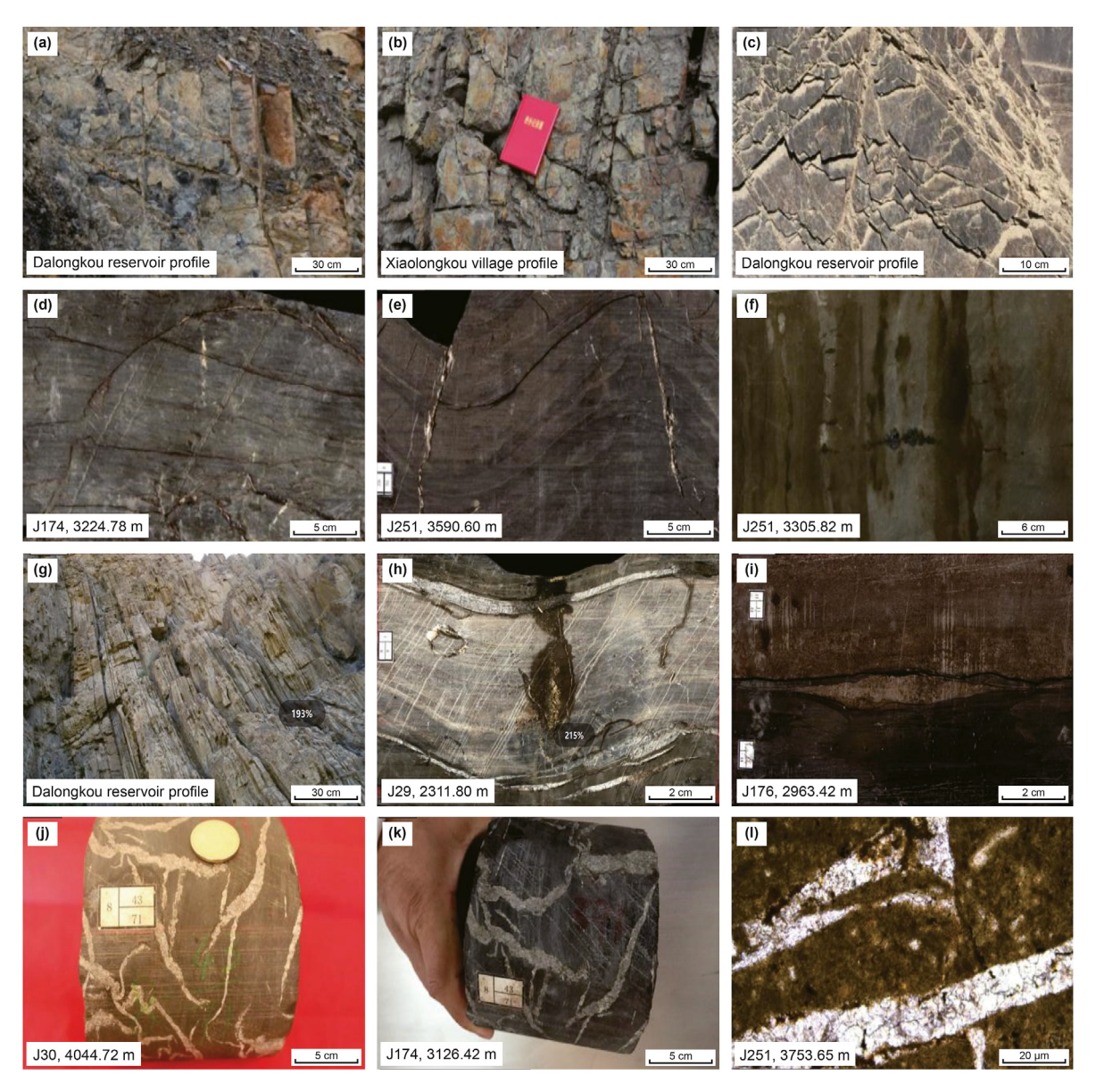


Fig. 2. Photographs of fractures (**a, b**) Shear fractures in outcrop. (**c**) Extensional fractures in outcrop. (**d**) Shear fractures in core from Well J174, 3223.31 m. (**e, f**) Extensional fractures in core from Well J251, 3590.60 and 3305.82 m. (**g**) Bedding fractures in outcrop. (**h**) Bedding fractures in core from Well J29, 2311.80 m. (**i**) Bedding fractures in core from Well J176, 2963.42 m. (**j**, **k**) Abnormal high-pressure fractures in cores from Well J30, 4044.72 m, and Well J174, 3126.42 m. (**l**) Pore-casted thin sections of core from Well J251, 3753.65 m (Fig. 2(e), 2(h), 2(j), 2(j), 2(k) and 2(l) are modified after Zhang et al., 2017; Fig. 2(b), 2(e) and 2(g) are modified after Kong et al., 2021).

- (a) Continuous high-permeability (high-conductivity) fractures. These fractures typically appear as black or dark sinusoids in FMI images owing to the presence of mud (Fig. 5(a)). They are prevalent and often appear in clusters in the tested section of Well J251.
- (b) Discontinuous high-permeability (high-conductivity) fractures. These fractures appear as discontinuous black or dark segments in FMI images (Fig. 5(b)) owing to mud invasion during drilling. The discontinuity of these high-permeability fractures may be attributed to diagenetic alteration of originally continuous high-permeability tectonic fractures, or to the formation of these fractures during diagenesis. In general, these discontinuous high-permeability fractures have low continuity and inter-fracture connectivity. Nevertheless, they can serve as effective migration pathways and improve reservoir permeability after being treated via acid fracturing. Determining the azimuths of these fractures can be challenging due to their discontinuous nature.
- (c) Low-permeability (high-resistivity) fractures. These fractures typically have low permeability because of the presence of high-resistivity mineral fillings such as calcite and quartz. They are represented by bright yellow or yellow sinusoidal lines in FMI images (Fig. 5(c)). Given the high degree of mineral filling, these fractures have limited storage capacity and permeability. However, as was the case for discontinuous high-permeability fractures, they can still serve as migration pathways and enhance reservoir permeability following acid fracturing treatment.

3.2.3. Fracture evaluation based on image logs

In addition to identifying fractures, image logs can be used to calculate the key parameters of fractures, such as length, density, aperture, permeability, and porosity (Table 4). Fracture identification based on image logs was conducted for Wells J28, J30, J32, J36, J174, and J251 in the Lucaogou Formation (Fig. S1). Correspondingly,

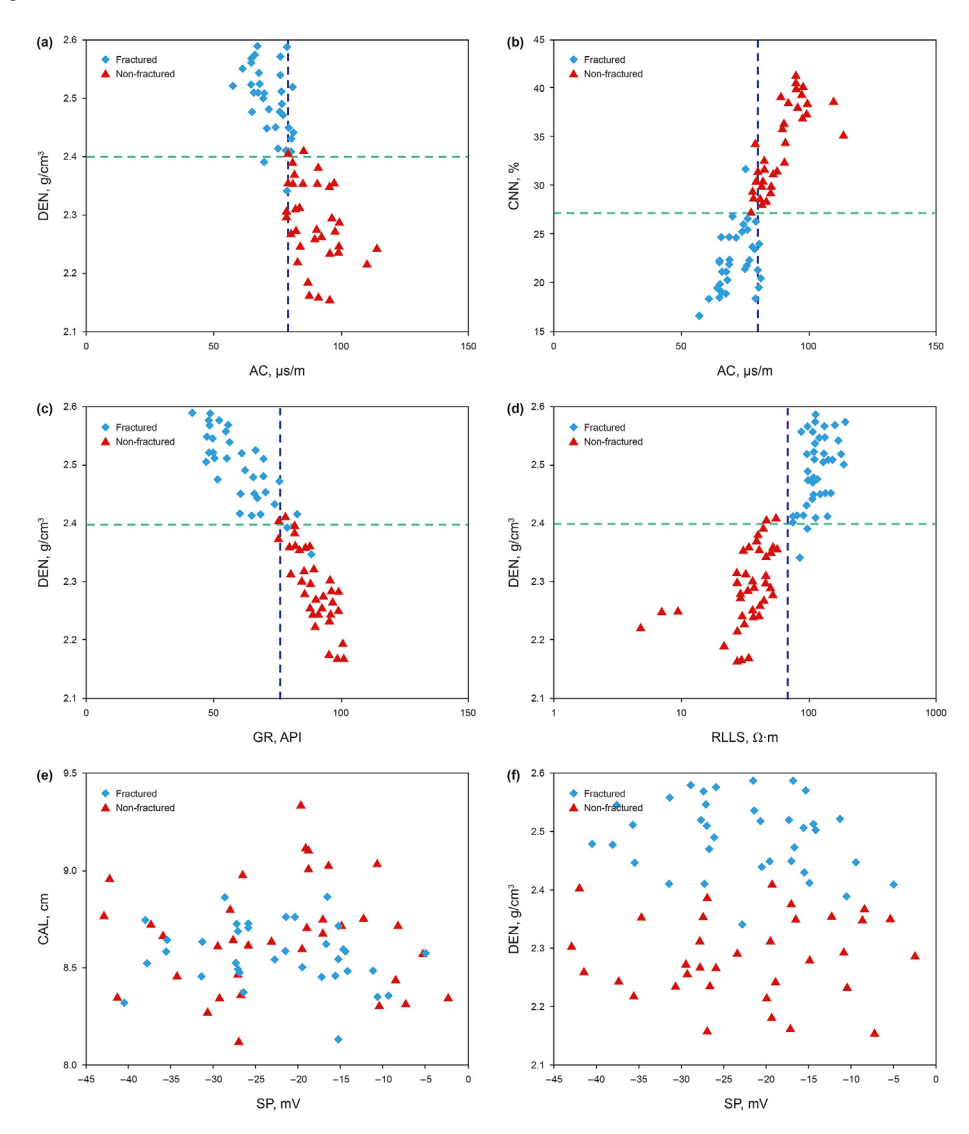


Fig. 3. Plots of data from conventional well logs. (a) Density (DEN) vs. acoustic (AC). (b) Compensated neutron log (CNL) vs. AC. (c) DEN vs. natural gamma log (GR). (d) DEN vs. shallow resistivity (RLLS). (e) Caliper (CAL) vs. spontaneous potential (SP). (f) DEN vs. SP.

the fracture parameters were calculated and analyzed statistically. We conclude that the upper and lower sweet-spot reservoirs $(P_2l_2^2)$ and $P_2l_1^2$) are favorable zones of fracture development in the Lucaogou Formation. Moreover, fracture development in the lower sweet spot $(P_2l_1^2)$ is superior to that in the upper sweet spot $(P_2l_2^2)$, with an average fracture density of 3.17 fractures/m, an average fracture length of 2.46 cm, and an average aperture of 0.25 mm. The 1st sand group of the 1st member of the Lucaogou Formation $(P_2l_1^1)$ exhibits fewer fractures. However, those fractures present are relatively wide, providing a certain amount of reservoir space. Considering this along with the imaging logging fracture evaluation, $P_2l_1^1$ could be viewed as the next favorable zone for fracture development following the upper and lower sweet spots.

3.3. Fracture development characteristics

3.3.1. Tectonic fractures

Based on the image logs from 10 wells (J33, J29, J30, J36, J32, J251, J172, J37, J22, and J31), the strike directions of tectonic fractures in each well are summarized in Fig. 6(a) and (b). The strike directions in the upper and lower sweet-spot reservoirs are largely consistent, indicating that fractures across different vertical layers of the Lucaogou Formation share a consistent tectonic history and

implying strong correlations between the stages of fracture formation. The tectonic fractures in the Lucaogou Formation strike mainly N–S, ENE–WSW, and NNW–SSE. The near N–S tectonic fractures occur mainly in the northern part of the Jimsar Sag, the ENE–WSW fractures are mainly in the middle and southern parts of the sag, and the NNW–SSE fractures are extensively developed across the entire sag.

3.3.2. Bedding fractures

Bedding fractures within the Lucaogou Formation are mainly horizontal, as shown by observations from field outcrops and drill cores. The fractures are distributed extensively throughout the entire Jimsar Sag. In the study area, the Lucaogou Formation comprises a complex of dark fine-grained saline-lake deposits. The rhythmic successions of beds within the formation are well-developed, providing the necessary materials for the formation of bedding fractures. These bedding fractures were identified and further analyzed at multiple scales using a combination of field observations, drill cores, and FMI images (Fig. 7), focusing on their characteristics and their influence on reservoir properties. In the dolomitic—sandy flat and dolomitic—muddy flat subfacies of the Lucaogou Formation, dissolution pores and fractures commonly occur along bedding planes, indicating the significant influence of

FMI imaging features	Image features 0° 90° 180° 270° 360°	Response features	Seismic interpretation
		Thick dark sections	Mudstone
Blocky		Thick yellow sections	Sandstone
		Thick bright sections	Limestone
Banded		Parallel high-conductivity anomalies	Layer interface
Ballueu		High-conductivity band with no notable width variation	Muddy band
		Bright sinusoid	Fracture with calcareous fillings
Linear		Black sinusoid	Fracture filled with pyrite
		Dark sinusoid with notable width variation	Fracture with argillaceous fllings or un-filled fracture
		Irregular jagged curve	Stylolite
Others		Symmetric orthogonal bar	Elliptical borehole
		Feathery or en echelon sinusoid	Drilling disturbance

Fig. 4. FMI characteristics of different types of fracture in the shale reservoir of the Lucaogou Formation (modified after Liu et al., 2019).

dissolution processes on the formation of dissolution-origin bedding fractures. The sandy bar, distal bar, sheet sand, and mudstone of the shore—shallow lake facies display well-developed bedding fractures, most of which occur in the shore—shallow lake mudstone. In the sandy bar facies, the bedding fractures frequently intersect high-angle tectonic fractures to form fracture networks.

Lucaogou Formation in the Jimsar Sag, with an emphasis on its shale reservoirs. Drill core samples were obtained between 2019 and 2021, ensuring a comprehensive dataset representative of the study area. These data points provide robust support for analyzing fracture characteristics and their spatial distribution.

4. Materials and methods

Quantifying the various parameters of fractures in shale reservoirs is essential to better understand the key factors that control fractures and predict their distribution. We conducted a detailed investigation of fracture parameters in the study area's shale reservoirs by undertaking statistical analyses of observations from various sources such as field outcrops, drill cores, thin sections, and well logs from 22 wells. The samples were collected from the

4.1. Fracture dip angle

The dip angles of fractures can be calculated accurately using imaging logs. Fractures that cut across wells exhibit a consistent morphology and appear as sinusoidal patterns in FMI images. The angle of the sinusoidal valley corresponds to the fracture dip angle, and the amplitude of the sinusoid can be used to determine the specific dip angle value (Zeng et al., 2010), as follows:

C. Zhang, Z.-Q. Hu, X.-Y. Kong et al. Petroleum Science 22 (2025) 2660–2676

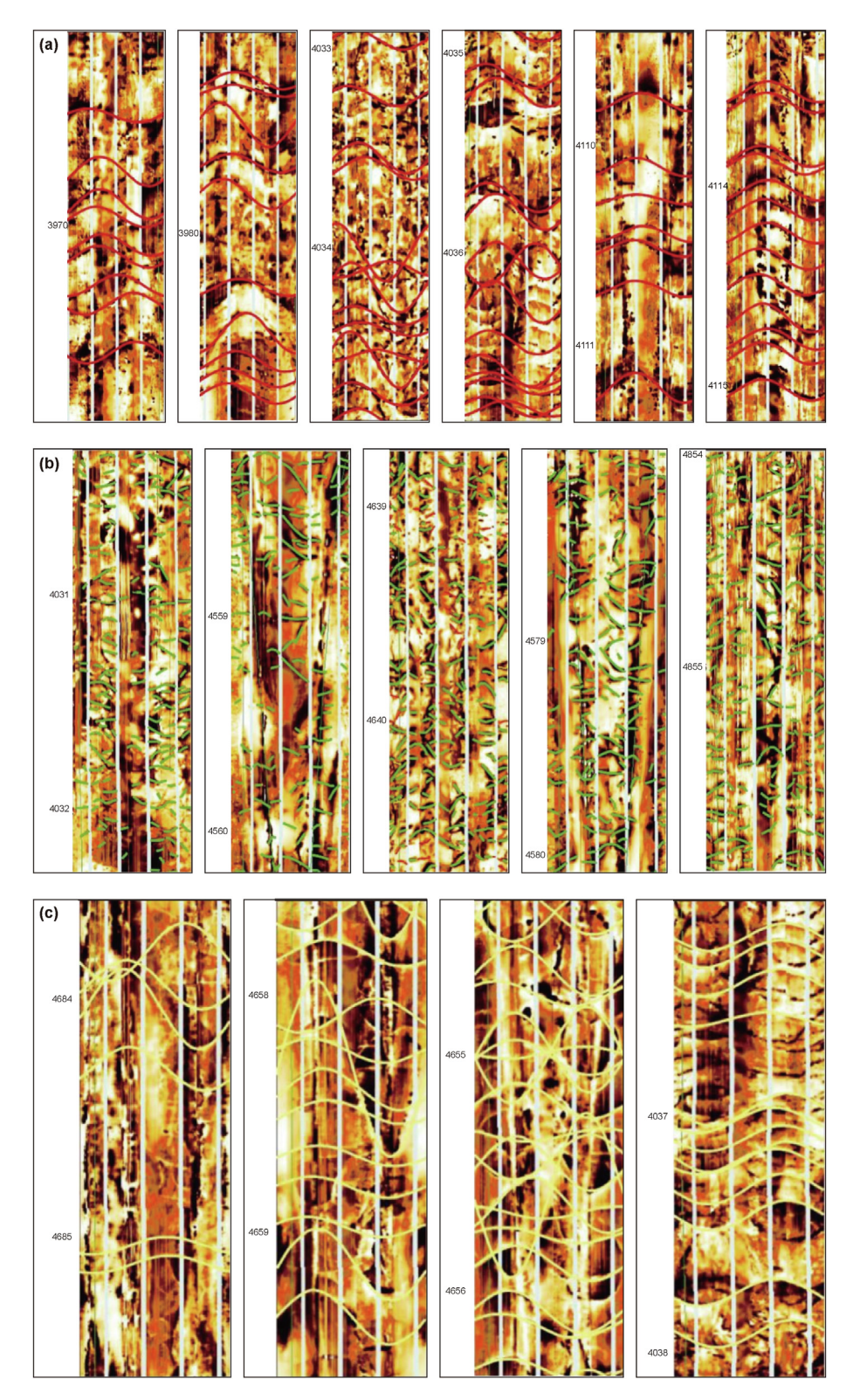


Fig. 5. (a) FMI of continuous high-permeability fractures in core from Well J251. (b) FMI of discontinuous high-permeability fractures in core from Well J251. (c) FMI of continuous low-permeability fractures in core from Well J251.

$$\theta = \arctan \frac{h}{d} \tag{1}$$

where θ is the fracture dip angle, h is the sinusoid amplitude, and d is the borehole diameter.

4.2. Fracture density

Fracture density and spacing are crucial indicators of the spatial distribution and concentration of fractures within a reservoir. By analyzing image logs, tectonic fractures and bedding fractures in the Lucaogou Formation were identified in 14 wells (J172, J173, J174,

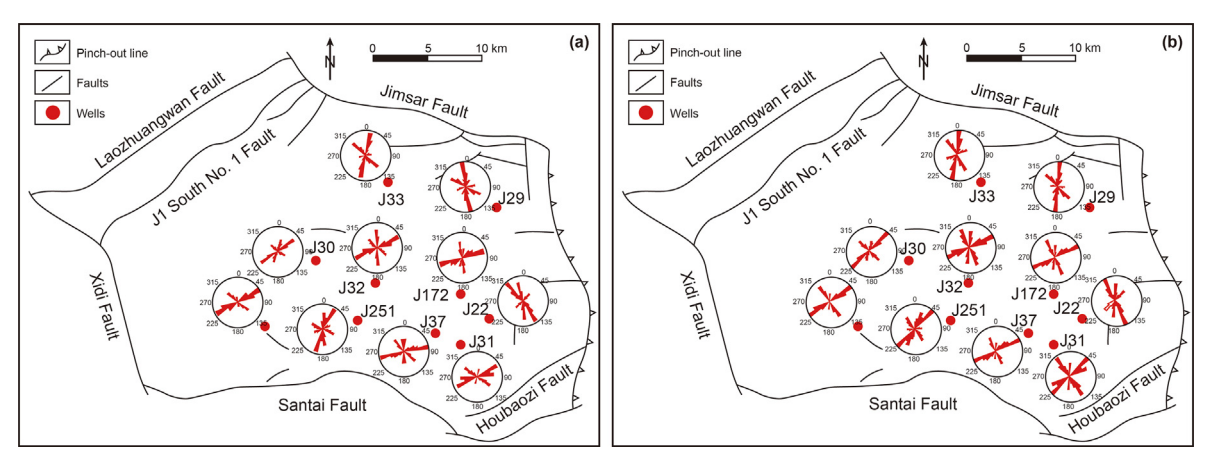


Fig. 6. (a) Rose diagrams showing the strike directions of tectonic fractures in the (a) upper and (b) lower sweet spots.

J22, J23, J25, J27, J29, J30, J31, J32, J34, J36, and J37), allowing for the computation of their linear densities.

4.3. Fracture aperture and filling

Precise determination of fracture aperture is essential for evaluating fracture permeability and gaining a comprehensive understanding of subsurface fluid flow. However, it is essential to recognize that the measured fracture aperture in drill cores may

not represent the actual aperture distribution in the underground environment. Therefore, appropriate corrections need to be applied to account for the *in situ* stress field conditions. One commonly used method involves estimating fracture aperture based on the amplitude difference between RLLD and RLLS logs (Sibbit and Faivre, 1989), as follows.

(1) For high-angle fractures (dip angles >75°), the fracture aperture is calculated as below:

Sedimentary facies	Lithological association	Main rock types	Fractures in cores	Fracture pattern diagram	Fracture characteristics
Dolomitic- sandy flat		Siltstone Siltstone			Bedding-parallel dissolution fractures and pores show bead-string-like distribution, and part of them intersect structural fractures to form fracture networks.
Dolomitic- muddy flat		Siltstone Siltstone			With certain apertures and partially mineral-filled, dissolution fractures and pores occur mainly along weak bedding planes.
Sandy bar	7 · · · · · · · · · · · · · · · · · · ·	Siltstone			The density of bedding fractures is high in thin layers, and most of them intersect structural fractures to form fracture networks.
Distal bar		Siltstone Siltstone			Bedding fractures are well developed, while structural fractures occur between bedding fractures and are isolated from bedding fractures.
Sheet sand		Sandy siltstone			Due to thin beds and cumulative thickness of sheet sand, bedding fractures are highly developed with bedding-parallel extensions. High-angle structural fractures are small in scale.
Mudstone of shore-shallow lake facies		Mudstone			Bedding fractures are the most developed. Straight fractures and dissolution fractures both occur and show no intersection with structural fractures.
	Siltstone	Dolomite	 Mudstone	Limestone	Limy siltstone

Fig. 7. Differentiated development of typical bedding fractures in different sedimentary facies.

$$e_{\rm v} = \left[\left(\frac{1}{R_{\rm LLS} - R_{\rm LLD}} \right) \cdot \frac{10^4}{4} \right] R_{\rm mf} \tag{2}$$

(2) For medium-to low-angle fractures (dip angles <75°), the fracture aperture is calculated as below:

$$e_{\rm h} = \left[\left(\frac{1}{R_{\rm LLS} - R_{\rm LLD}} \right) \cdot \frac{10^4}{1.2} \right] R_{\rm mf} \tag{3}$$

where $R_{\rm LLD}$ is the resistivity value of the RLLD log, $\Omega \cdot$ m; $R_{\rm LLS}$ is the resistivity value of the RLLS log, $\Omega \cdot$ m; $R_{\rm mf}$ is the resistivity of mud filtrate, $\Omega \cdot$ m; and $e_{\rm v}$ and $e_{\rm h}$ are the fracture aperture, μ m.

Fracture fillings were investigated to determine the extent of fracture filling and their types and characteristics.

4.4. Fracture porosity

Fracture porosity refers to the volumetric fraction of fracture space to the total rock volume (Lv et al., 2016). Although core data provide valuable insights into fracture characteristics within a layer, relying solely on parameters derived from measurements of fracture lengths and apertures may introduce errors. Therefore, estimations of fracture porosity based solely on core measurements are insufficient. However, during drilling, mud filtrate infiltrates fractures, which allows for the calculation of fracture porosity using well logs. In most cases, the dual laterolog resistivity is used for this purpose (Deng, 2009), as follows:

$$\theta_{\rm f} = mf \sqrt{R_{\rm mf} \left(\frac{1}{R_{\rm LLS}} - \frac{1}{R_{\rm LLD}}\right)} \tag{4}$$

where θ_f is fracture porosity, %, mf is the fracture porosity index, $R_{\rm mf}$ is the mud filtrate resistivity $(\Omega \cdot {\rm m})$, $R_{\rm LLD}$ is the resistivity of the RLLD log $(\Omega \cdot {\rm m})$, and $R_{\rm LLS}$ is the resistivity of the RLLS log, $\Omega \cdot {\rm m}$.

The value of $R_{\rm mf}$ should correspond to the mud filtrate resistivity at the formation temperature, which requires conversion from the resistivity measured at normal temperature. The necessary data for this calculation include the surface mud filtrate resistivity, the surface and formation temperature, and the depths of the layers of interest in the well (obtained from drilling data). The corresponding formulae are as follows:

$$R_{\rm mf2} = \left(\frac{t_1 + 21.5}{t_2 + 21.5}\right) \times R_{\rm mf1} \tag{5}$$

$$t_2 = KD + t_1 \tag{6}$$

where $R_{\rm mf1}$ is the surface mud filtrate resistivity, $\Omega \cdot$ m; $R_{\rm mf2}$ is the mud filtrate resistivity under formation conditions; $\Omega \cdot$ m; t_1 is the surface temperature at which $R_{\rm mf1}$ is measured, °C; t_2 is the formation temperature, °C; D is the layer depth, m; and K is the geothermal gradient, which is computed using the temperature at the bottom of the hole and the well depth.

4.5. Fracture permeability

Fracture permeability is an important parameter for characterizing the degree of development of a fracture. A higher fracture permeability generally implies well-developed natural fractures (Fan and Liu, 2019; Zhang et al., 2019). The permeability of fractures (K_f) within a shale reservoir is in direct proportion to the

fracture aperture and fracture porosity (Zhou, 2006) and can be expressed mathematically as follows:

$$K_{\rm f} = 0.2775 \times \varepsilon^2 \times \phi_{\rm f} \tag{7}$$

where $K_{\rm f}$ is the fracture permeability, $10^{-3}~\mu{\rm m}^2$; $\phi_{\rm f}$ is the fracture porosity based on well logging, %; and ε is the fracture aperture, $\mu{\rm m}$.

5. Results and discussion

5.1. Fracture dip angle

The analysis of image logs from 14 wells (J172, J173, J174, J22, J23, J25, J27, J29, J30, J31, J32, J34, J36, and J37) reveals the dominance of medium-to high-angle fractures within the study area. Specifically, the near N–S and NNW–SSE fractures have higher dip angles, averaging 78.6° and 72.7°, respectively, whereas the ENE–WSW fractures have lower dip angles, averaging 35.8° (Fig. S2).

5.2. Fracture density

Analysis of representative wells indicates that there are wide variations in the linear density of the tectonic fractures (Fig. 8(a)). Wells J174, J23, J25, J36, and J37 display higher linear densities, all surpassing 0.8 fractures/m. Of these wells, J174 and J36 exhibit the most pronounced development of tectonic fractures, with linear densities reaching 1.72 and 1.69 fractures/m, respectively.

Similarly, the linear densities of bedding fractures in the studied wells vary markedly (Fig. 8(b)). Wells J172, J174, J23, J29, J36, and J37 have high bedding-seam linear densities, all exceeding 2.5 fractures/m. Of these wells, J36 has the highest bedding-seam linear density of 3.42 fractures/m.

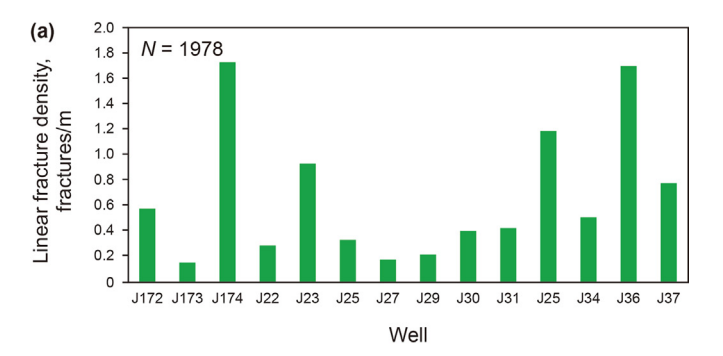
As shown in Fig. 8(c), wells J172, J174, J23, J29, J25, J36, and J37 display relatively high total fracture densities and exceed 3 fractures/m. Wells J36 and J174 have the greatest fracture development, with fracture densities of 5.12 and 4.55 fractures/m, respectively.

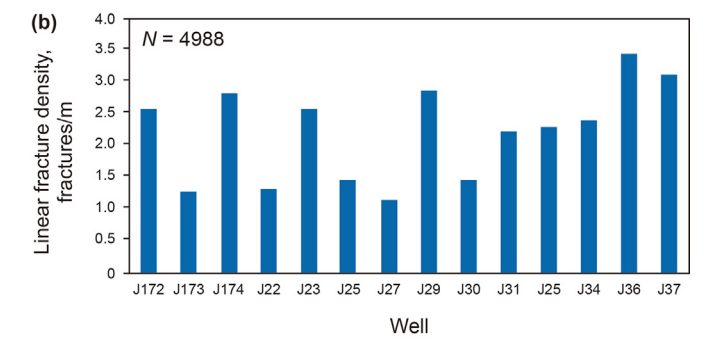
Fracture planar density is also an important parameter for characterizing fracture development in shale oil reservoirs. For the selected representative wells, the fracture planar density of the upper sweet spot averages 0.71 m/m², whereas that of the lower sweet spot averages 0.91 m/m² (Fig. 9). Overall, the fracture planar density of the lower sweet spot is higher than that of the upper sweet spot.

5.3. Fracture aperture and filling

Our calculations show that the apertures of the bedding fractures within the Lucaogou Formation are generally small (typically <0.1 mm), whereas those of the tectonic fractures are mainly 0.05–0.8 mm (average 0.46 mm), with 77.5% of such fractures having apertures of <0.4 mm. Notably, 52.3% of the tectonic fractures have apertures below 0.2 mm (Fig. 10).

Analysis of drill cores from various wells in the Jimsar Sag reveals that fracture fillings in the target layers are composed mainly of calcite and quartz, with local occurrences of argillaceous materials (Fig. 11(a) and (b)). Furthermore, early formed fillings have undergone substantial modification through subsequent dissolution processes. Well data from across the study area indicate that the fractures exhibit limited filling. Unfilled fractures within the upper and lower sweet spots account for 66.8% and 68.2% of the total fractures, respectively (Fig. 11(c) and (d)). This situation is favorable for fluid flow and accumulation. The small apertures and limited filling of bedding fractures, combined with the relatively larger apertures of tectonic fractures, suggest that these fractures





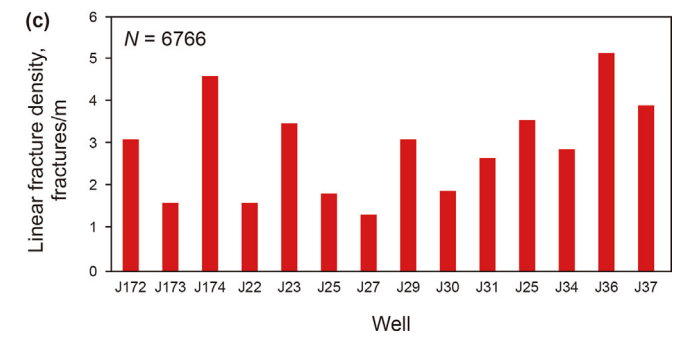


Fig. 8. Histograms of linear (a) tectonic and (b) bedding fracture densities in the Lucaogou Formation in representative wells of the Jimsar Sag, Junggar Basin. (c) Histogram of total fracture densities (bedding fractures and tectonic fractures).

play complementary roles in hydrocarbon migration and accumulation. Bedding fractures provide pathways for lateral fluid migration due to their extensive horizontal connectivity, while tectonic fractures, with their higher vertical permeability, facilitate vertical fluid flow. The dissolution-modified fillings further enhance fracture permeability by creating secondary pore spaces. These characteristics collectively improve the efficiency of hydrocarbon flow within the reservoir, making the Lucaogou Formation a favorable target for shale oil development.

5.4. Fracture porosity and permeability

We performed fracture porosity calculations using the above formulae and well logging data from 20 wells in the Lucaogou Formation (J22, J23, J24, J25, J27, J28, J29, J30, J31, J32, J33, J34, J35, J36, J37, J172, J173, J174, J176, and J251). We obtained average fracture porosity values for the upper and lower sweet spots and all fractures for each well (Fig. 12(a)). Across all wells, the average fracture porosity of the lower sweet spot is higher than that of the upper sweet spot. Moreover, the average fracture porosity is relatively high in wells J22, J25, J27, J30, J32, and J34, with all values surpassing 0.2%; well J27 has the highest average fracture porosity

(0.24%; Fig. 12(a)). The relationship between fracture porosity and well depth (Fig. 12(c)) demonstrates that the fracture porosity in the study area ranges from 0.001% to 0.045%. The upper and lower sweet spots ($P_2l_2^2$ and $P_2l_1^2$) exhibit considerably higher fracture porosities than other parts of the wells, and the porosity of the lower sweet spot is generally higher than that of the upper sweet spot.

Using the above formulae and the well logging data, the average fracture permeability of the upper and lower sweet spots and all fractures was calculated for 20 wells (J22, J23, J24, J25, J27, J28, J29, 30, 31, 32, 33, 34, 35, 36, 37, 172, 173, 174, 176, and 1251; Fig. 12(b)). Consistent with the trend observed for fracture porosity, the average fracture permeability of the lower sweet spot is notably higher than that of the upper sweet spot for all wells. Wells with elevated average fracture permeabilities include J30, J32, and J173, with all values surpassing $20 \times 10^{-3} \mu m^2$. Well J34 yields a maximum value of 25.38 \times 10⁻³ μ m² is reached. Analysis of the relationship between fracture permeability and well depth (Fig. 12(d)), indicates that fracture permeability ranges from 2.56×10^{-3} to 33.88×10^{-3} µm², and the upper and lower sweet spots $(P_2l_2^2$ and $P_2l_1^2)$ yield considerably higher values. Moreover, there is a positive correlation between fracture permeability and fracture porosity, and the lower sweet spot has a much higher fracture permeability than the upper sweet spot. The values for both fracture porosity and fracture permeability indicate that natural fractures are more extensively developed in the lower sweet spot than in the upper sweet spot, which is consistent with core observations.

5.5. Novel rose diagram method for fracture characterization

Fractures provide vital spaces for hydrocarbon migration and storage in shale oil reservoirs. Traditionally, rose diagrams have been employed to characterize fracture parameters, focusing primarily on the occurrence of fractures. However, this conventional method of representation fails to incorporate other fracture characteristics such as dimension, degree of filling, and density. To address this limitation, we developed a novel method of fracture representation, which captures multiple fracture parameters including dip directions and angles, lengths, apertures, degrees of filling, the linear densities of fractures, and strike directions. The new method facilitates comprehensive multi-parameter characterization of the fractures.

Eight parameters across four elements were selected to represent the characteristics of fractures in the shale reservoirs using the novel rose diagram. These elements include the occurrence, scale, filling, and degrees of development of the fractures.

The novel rose diagram, based on the conventional rose diagram for joints, incorporates the parameters of three additional elements to characterize the key parameters of fractures (Fig. 13(a)). The new parameters are the scale of the fracture (average fracture length and aperture), the fracture filling (filling types and degrees of filling), and the degree of fracture development (linear fracture density).

First, the azimuth circle is divided into 36 identical sectors (each corresponding to 10°) to represent the strike direction of fractures. The sectors within the upper half circle depict the dominant range of strike directions, the average linear density, the degree of filling, and mineral types for a group of fractures. The start and end of each sector indicate the dominant range of strike directions for the respective fracture group. The radius of the sector represents the average linear fracture density, with the corresponding value marked on the arc of the sector (Fig. 13(a)). The inside of the sector is filled with different shades, representing various minerals and degrees of filling.

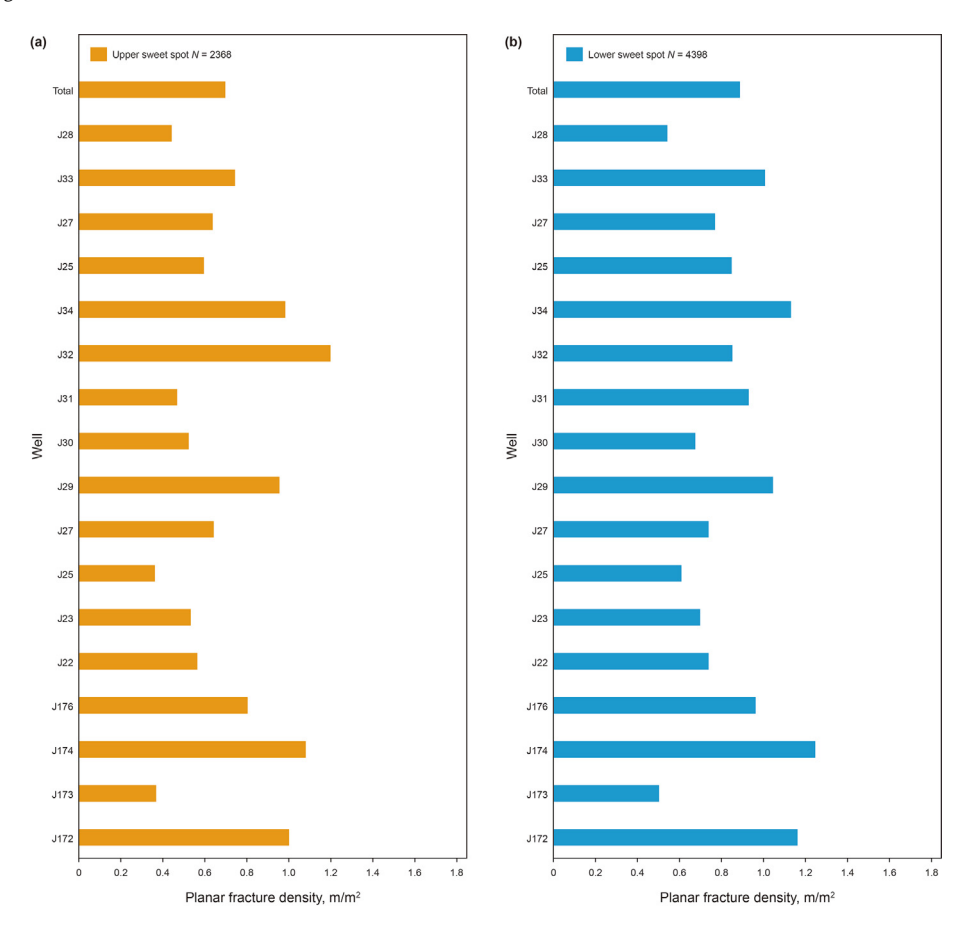


Fig. 9. Fracture planar density distributions in the (a) upper and (b) lower sweet spots.

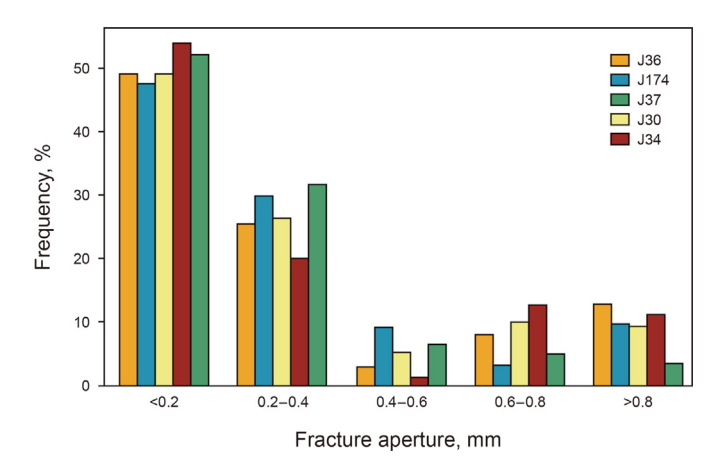


Fig. 10. Distributions of tectonic fracture apertures in representative wells.

In the lower half circle, each spoke represents the average aperture ("b"), length ("c"), and dip angle ("d") of the fracture group, corresponding to the sectors in the upper half circles. The length of the spoke (circle radius) corresponds to the average fracture length ("b"), and an arrow on the spoke indicates the dip direction of the fracture.

The novel rose diagram generated to represent the fractures within the Lucaogou Formation using the derived fracture parameters and methods described above is shown in Fig. 13(b). This diagram effectively portrays all key fracture parameters.

Three groups of tectonic fracture are developed in the Lucaogou Formation, striking ENE—WSW (A), approximately N—S (B), and

NNW—SSE (C). The linear fracture density represents the degree of fracture development; therefore, the NNW—SSE tectonic fractures have an average linear density of 0.96 fractures/m, the N—S fractures have a value of 1.34 fractures/m, and the ENE—WSW fractures have a value of 1.65 fractures/m. The average fracture apertures of the ENE—WSW, N—S, and NNW—SSE tectonic fractures are 8.7, 7.6, and 6.2 cm, respectively. The N—S and NNW—SSE tectonic fractures are high-angle fractures with average dip angles of 78.6° and 72.7°, respectively, whereas the ENE—WSW tectonic fractures are low-angle, with an average dip of 35.8°. The ENE—WSW tectonic fractures have the highest proportions of unfilled fractures. Overall, the ENE—WSW (Group A) tectonic fractures are the most highly developed fractures in the Lucaogou Formation of the Jimsar Sag.

This novel method can also be utilized for quantitative characterization of tectonic fractures in the target layers of individual wells. Novel rose diagrams for the Lucaogou Formation were generated for nine wells within the Jimsar Sag (J28, J32, J32, J33, J251, J5, J18, J15, J6, and J7), and they provide valuable insights into the main parameters and status of development of tectonic fractures within each of these wells. Statistical analyses revealed significant differences in dip directions and angles, fracture lengths, apertures, degrees of filling, and the linear densities of tectonic fractures across the wells. Overall, the ENE—WSW tectonic fractures are the most highly developed (Fig. 13(c)).

Fractures with the same general characteristics can have markedly different effects on the development of shale reservoirs and the formation of shale oil. Based on production statistics for the Jimsar Sag, the distribution of the average daily oil production for eight wells was mapped by Zhang et al. (2022). At the northern end of well-developed N—S-striking fractures, well production is

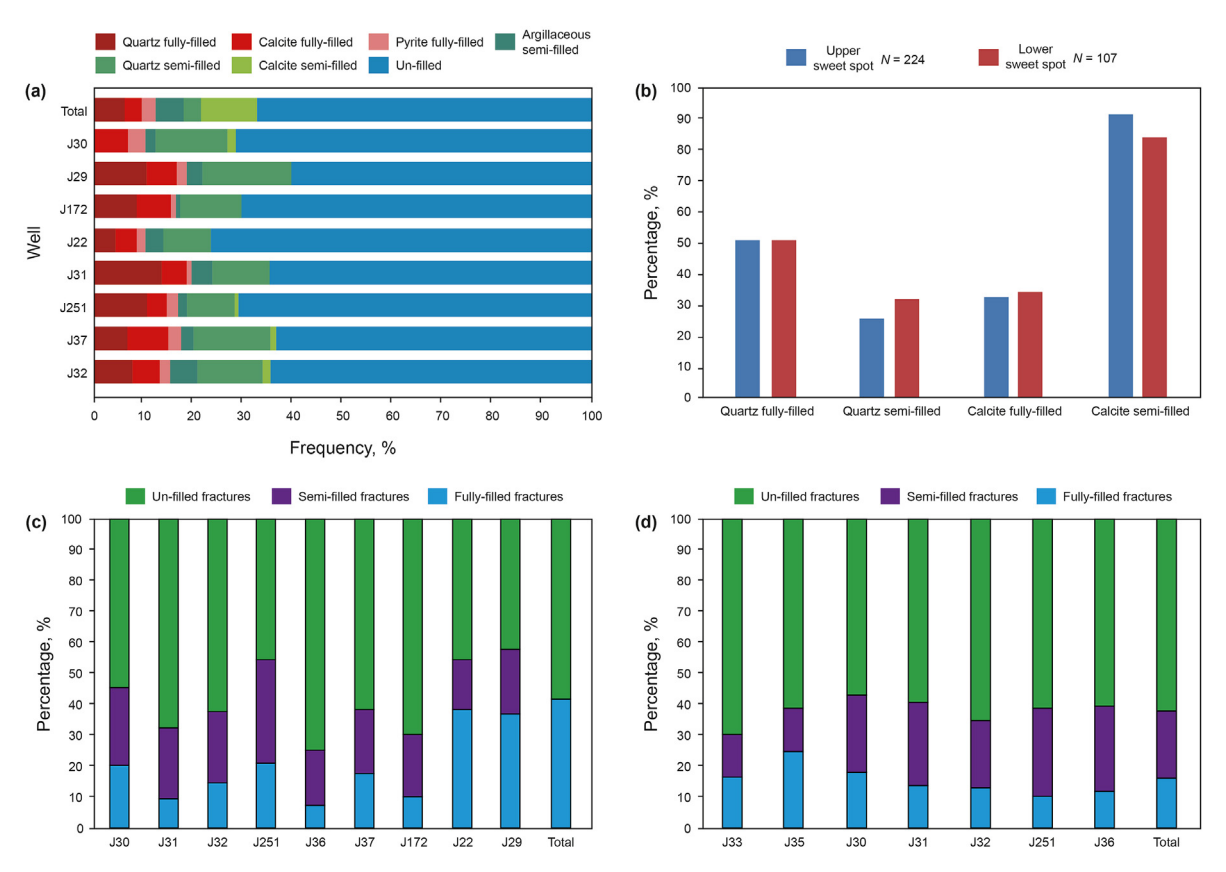


Fig. 11. (a) Histogram of types and degrees of filling in fractures. (b) Mineral filling characteristics. (c) Statistics of fracture fillings in the upper sweet spot. (d) Statistics of fracture fillings in the lower sweet spot.

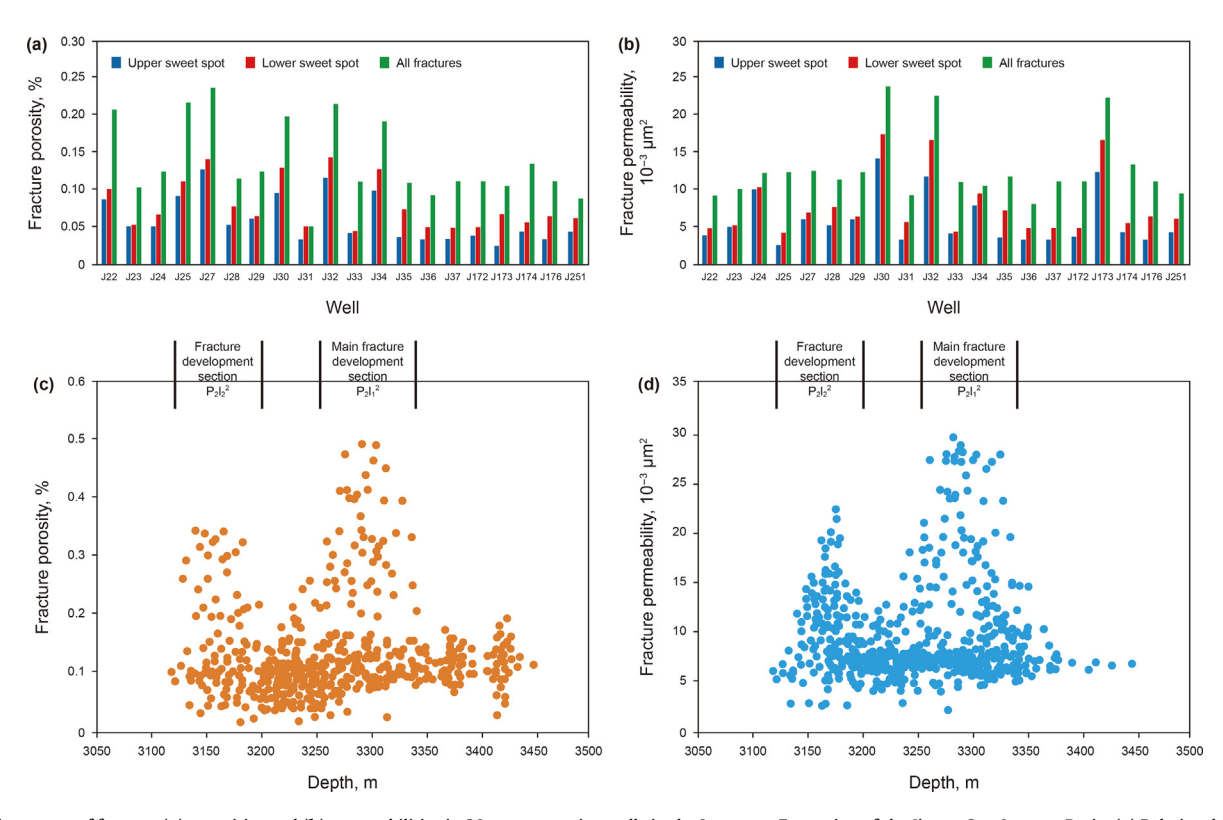


Fig. 12. Histograms of fracture (a) porosities and (b) permeabilities in 20 representative wells in the Lucaogou Formation of the Jimsar Sag, Junggar Basin. (c) Relationship between fracture permeabilities and depth in the wells.

C. Zhang, Z.-Q. Hu, X.-Y. Kong et al.

Petroleum Science 22 (2025) 2660–2676

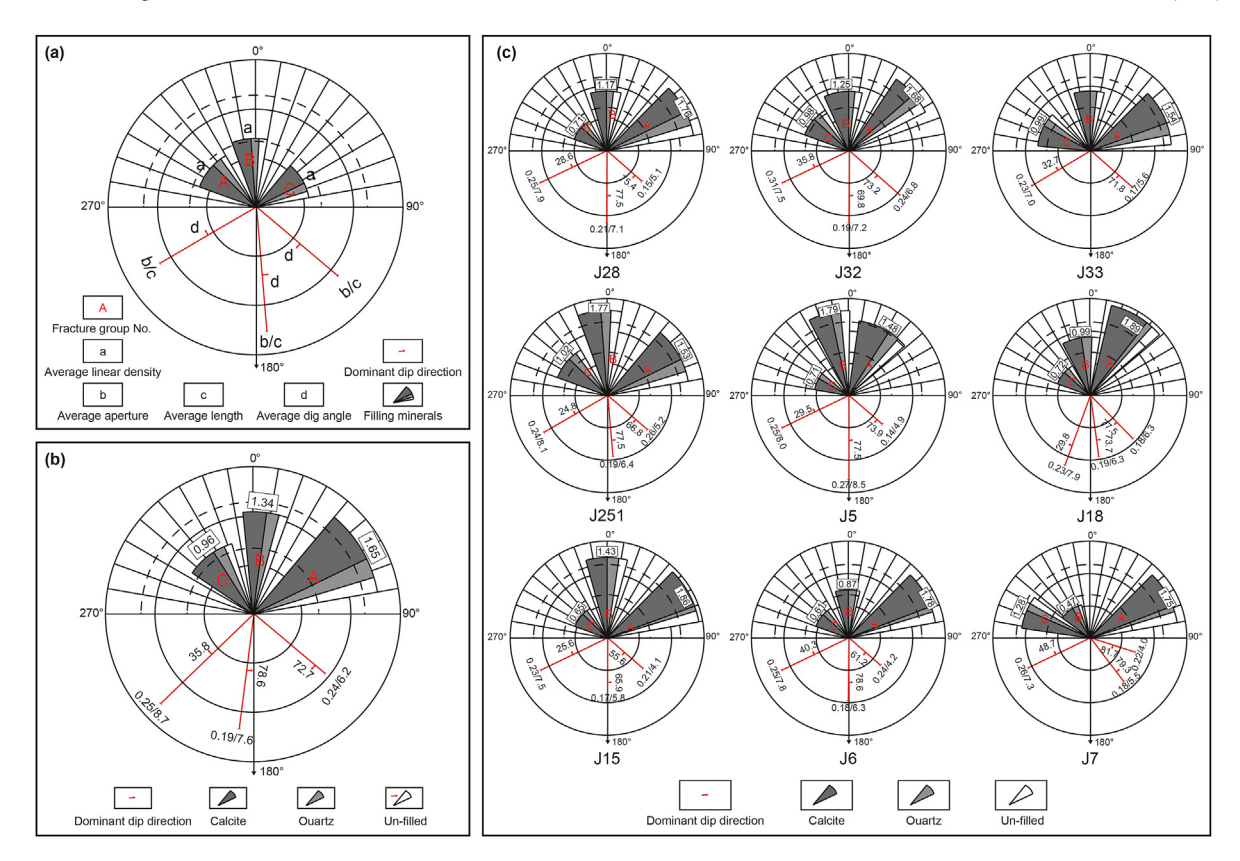


Fig. 13. (a) Novel rose diagram for characterizing key fracture parameters. (b) Novel rose diagram representing key fracture parameters. (c) Novel rose diagrams of fractures in wells J28, J32, J33, J251, J5, J18, J15, J6, and J7.

relatively low, whereas it is relatively high in the southern part of the sag, where well-developed ENE—WSW- and NNW—SSE-striking fractures occur.

6. Conclusions

- (1) The natural fractures within the shale reservoirs of the Permian Lucaogou Formation in the Jimsar Sag can be categorized into three types: tectonic, diagenetic, and abnormal high-pressure fractures.
- (2) Conventional well logs provide insights into the characteristics of these shale reservoirs. Fractured sections exhibit higher GR, AC, and CNL and lower RLLS and DEN values compared with non-fractured sections. However, there are no significant differences in SP and CAL values between the fractured and non-fractured sections. Fractured sections typically have GR counts of >75 API, shallow laterolog resistivities of $< 80 \ \Omega \cdot m$, neutron densities of $< 2.40 \ g/cm^3$, neutron porosities of >27%, and interval transit times of >23.77 µs/m. Imaging logging revealed diverse natural fractures that can be categorized as having continuous highpermeability, discontinuous high-permeability, and discontinuous low-permeability, based on resistivity measurements.
- (3) The tectonic fractures in shale reservoirs exhibit apertures ranging from 0.05 to 0.4 mm. N—S and NNW—SSW fractures have relatively high dip angles (78.6° and 72.7°, respectively), while ENE—WSW fractures exhibit lower dip angles (35.8°). Bedding fractures are nearly horizontal with apertures smaller than 0.1 mm. ENE—WSW fractures show the highest linear density (1.65 fractures/m) and the largest proportion

- of unfilled fractures. Fracture porosities and permeabilities are higher in the sweet spots, with the lower sweet spot exhibiting a greater degree of fracture development.
- (4) The novel rose diagram method enables multi-parameter characterization of fractures, including orientation, aperture, density, and filling degree. Its application to the Lucaogou Formation has revealed the fracture characteristics and their impact on reservoir performance, providing a robust framework for enhancing reservoir evaluation accuracy and optimizing the development strategies for unconventional hydrocarbon resources.

CRediT authorship contribution statement

Chen Zhang: Writing — review & editing, Writing — original draft, Formal analysis, Data curation, Conceptualization. **Zong-Quan Hu:** Investigation, Funding acquisition, Data curation. **Xiang-Ye Kong:** Funding acquisition, Data curation, Conceptualization. **Bo Gao:** Project administration, Investigation, Funding acquisition. **Jia-Yi Liu:** Software, Methodology, Investigation. **Yu-Han Huang:** Resources, Methodology, Funding acquisition. **Hua-Dong Chen:** Visualization, Project administration, Methodology.

Declaration of interests

The authors declare that they have no known competing financial interests or personal relationships that could have appeared to influence the work reported in this paper.

Acknowledgments

Chen Zhang and Xiang-Ye Kong contributed equally to this work. This work was supported by grants from the National Natural Science Foundation of China (Nos. 42002050 and 42072174).

Appendix A. Supplementary data

Supplementary data to this article can be found online at https://doi.org/10.1016/j.petsci.2025.03.022.

References

- Cao, Y., Zhu, N., Zhang, S., Xi, K., Xue, X., et al., 2019. Diagenesis and reserving space characteristics of tight oil reservoirs of permian Lucaogou Formation in jimusar sag of Junggar Basin, China. J. Earth Sci. Environ. 41 (3), 253–266 (in Chinese).
- Curtis, J.B., 2002. Fractured shale-gas systems. AAPG Bull. 86 (11), 1921–1938. https://doi.org/10.1306/61EEDDBE-173E-11D7-8645000102C1865D.
- Clarkson, C.R., Solano, N., Bustin, R.M., Bustin, A.M.M., Chalmers, G.R.L., He, L., et al., 2013. Pore structure characterization of North American shale gas reservoirs using USANS/SANS, gas adsorption, and mercury intrusion. Fuel 103, 606–616. https://doi.org/10.1016/j.fuel.2012.06.119.
- Chalmers, G.R., Bustin, R.M., Power, I.M., 2012. Characterization of gas shale pore systems by porosimetry, pycnometry, surface area, and field emission scanning electron microscopy/transmission electron microscopy image analyses: examples from the Barnett, Woodford, Haynesville, Marcellus, and Doig units. AAPG Bull. 96 (6), 1099–1119. https://doi.org/10.1306/10171111052.
- Deng, H., 2009. The Development and Assessment of Fault-Association Fracture System—A Case Study of Daleel Field in Oman. Chengdu University of Technology, master's thesis (in Chinese).
- Du, J., He, H., Li, J., Yang, T., Huang, F., Guo, B., et al., 2014. Progress in China's tight oil exploration and challenges. China Petrol. Explore (in Chinese).
- Dong, S., Ke, S., Zhang, H., Liu, C., 2013. On fracture identification with conventional well logging data. Well Logging Technol. 37 (4), 380–384+388 (in Chinese). https://doi.org/10.16489/j.issn.1004-1338.2013.04.010.
- Fall, A., Eichhubl, P., Bodnar, R.J., Laubach, S.E., Davis, J.S., 2015. Natural hydraulic fracturing of tight-gas sandstone reservoirs, Piceance Basin, Colorado. GSA Bull 127 (1-2), 61–75. https://doi.org/10.1130/B31021.1.
- Fall, A., Eichhubl, P., Cumella, S.P., Bodnar, R.J., Laubach, S.E., Becker, S.P., 2012. Testing the basin-centered gas accumulation model using fluid inclusion observations; southern Piceance Basin, Colorado. AAPG Bull. 96 (12), 2297–2318. https://doi.org/10.1306/05171211149.
- Fan, L., Liu, S., 2019. Fluid-dependent shear slip behaviors of coal fractures and their implications on fracture frictional strength reduction and permeability evolutions. Int. J. Coal Geol. 212, 103235. https://doi.org/10.1016/j.coal.2019.103235.
- Feng, Y., Xiao, X., Wang, E., Sun, J., Gao, P., 2021. Oil retention in shales: a review of the mechanism, controls and assessment. Front. Earth Sci. 9, 720839. https:// doi.org/10.3389/feart.2021.720839.
- Fu, J., Li, S., Niu, X., Deng, X., Zhou, X., 2020. Geological characteristics and exploration of shale oil in chang 7 member of triassic yanchang formation, ordos basin, NW China. Petrol. Explor. Dev. 47 (6), 931–945. https://doi.org/10.1016/s1876-3804(20)60107-0.
- Gale, J.F.W., Laubach, S.E., Olson, J.E., Eichubl, P., Fall, A., 2014. Natural fractures in shale: a review and new observations. AAPG Bull. 98, 2165–2216. https:// doi.org/10.1306/08121413151.
- Ghanizadeh, A., Clarkson, C.R., Aquino, S., Ardakani, O.H., Sanei, H., 2015. Petrophysical and geomechanical characteristics of Canadian tight oil and liquid-rich gas reservoirs: I. Pore network and permeability characterization. Fuel 153, 682–691. https://doi.org/10.1016/j.fuel.2015.02.113.
- Hong, Y., 1998. Logging Principles and Comprehensive Interpretation. China Univ. Petrol. Press, Dongying (in Chinese).
- Jia, C., Zheng, M., Zhang, Y., 2012. Unconventional hydrocarbon resources in China and the prospect of exploration and development. Petrol. Explor. Dev. 39 (2), 139–146. https://doi.org/10.1016/S1876-3804(12)60026-3.
- Kong, X., Zeng, J., Tan, X., et al., 2021. Natural tectonic fractures and their formation stages in tight reservoirs of Permian Lucaogou Formation, Jimsar Sag, southern Junggar Basin, NW China. Marine and Petroleum Geology 133, 105269. https:// doi.org/10.1016/j.marpetgeo.2021.105269.
- Kuang, L., Tang, Y., Lei, D., Chang, Q., Ouyang, M., Hou, L., et al., 2012. Formation conditions and exploration potential of tight oil in the Permian saline lacustrine dolomitic rock, Junggar Basin, NW China. Petrol. Explor. Dev. 39 (6), 700–711. https://doi.org/10.1016/S1876-3804(12)60095-0.
- Laubach, S.E., Fall, A., Copley, L.K., Marrett, R., Wilkins, S.J., 2016. Fracture porosity creation and persistence in a basement-involved laramide fold, upper cretaceous frontier formation, green river basin, USA. Geol. Mag. 153 (5-6), 887–910. https://doi.org/10.1017/s0016756816000157.
- Laubach, S.E., Lander, R.H., Criscenti, L.J., et al., 2019. The role of chemistry in fracture pattern development and opportunities to advance interpretations of geological materials. Rev. Geophys. 57, 1065—1111. https://doi.org/10.1029/ 2019rg000671.

- Lu, S., Zhang, Y., Li, Q., Ju, Y., 2016. Nanotechnology and its application in the exploration and development of unconventional oil and gas. Bull. China Soc. Mineral Petrol. Geochem. 35 (1), 28–36 (in Chinese). https://doi.org/10.3969/j. issn.1007-2802.2016.01.003.
- Li, D., He, D., Yong, T., 2016. Reconstructing multiple arc-basin systems in the altai—Junggar area (NW China): implications for the architecture and evolution of the western central Asian Orogenic Belt. J. Asian Earth Sci. 121, 84–107. https://doi.org/10.1016/j.jseaes.2016.02.010.
- Liu, W., Zhang, C., Gao, G., Luo, C., Wu, W., Shi, X., et al., 2017a. Controlling factors and evolution laws of shale porosity in Longmaxi Formation, Sichuan Basin. Acta Petrol. Sin. 38 (2), 175–184. https://doi.org/10.7623/syxb201702005 (in Chinese).
- Liu, Y., Dong, X., Yan, L., Chen, F., Gao, Y., Chen, Z., et al., 2019. Quantitative characterization of pore structure of Lucaogou Formation in Jimsar sag. Xinjing Pet. Geol. 40 (3), 284–289 (in Chinese). https://doi.org/10.7657/XJPG20190305.
- Liu, D., Zhang, C., Pan, Z., Huang, Z., Luo, Q., Song, Y., et al., 2020. Natural fractures in carbonate-rich tight oil reservoirs from the Permian Lucaogou Formation, southern Junggar Basin, NW China: insights from fluid inclusion microthermometry and isotopic geochemistry. Mar. Petrol. Geol. 119, 104500. https:// doi.org/10.1016/j.marpetgeo.2020.104500.
- Liu, D., Zhang, C., Luo, Q., Zhang, Y., Gao, Y., Zhang, Y., et al., 2017b. Development characteristics and controlling factors of natural fractures in Permian Lucaogou Formation tight reservoir in Jimsar sag, Junggar Basin. China Petrol. Explore 22 (4), 36–47. https://doi.org/10.3969/j.issn.1672-7703.2017.04.004 (in Chinese).
- Liu, D., Yang, D., Zhang, Z., Zhang, C., Luo, Q., Pan, Z., et al., 2019. Fracture identification for tight reservoirs by conventional and imaging logging: a case study of Permian Lucaogou Formation in Jimsar Sag. Junggar Basin. Lithol. Reserv. 31 (3), 76–85. https://doi.org/10.12108/yxyqc.20190309.
- 76—85. https://doi.org/10.12108/yxyqc.20190309.
 Lv, H., Lu, Y., Cui, Y., Li, X., Wang, R., Zheng, Y., 2016. Improved porosity model for fluid nature and fracture porosity evaluation. J Appl. Acoust. 35 (4), 351—356. https://doi.org/10.11684/j.issn.1000-310X.2016.04.010 (in Chinese).
- Ma, K., Hou, J., Yan, L., Chen, F., 2018. Pore-throat structures and their control of terrestrial lacustrine tight reservoir quality: the Permian Lucaogou Formation, Jimsar Sag, northwestern China. Interpretation 6 (4), T889—T906. https:// doi.org/10.1190/INT-2017-0209.1.
- Ma, K., Liu, Y., Hou, J., Huang, S., Yan, L., Chen, F., et al., 2019. Densification mechanism of tight reservoirs from mixed sedimentation in saline lacustrine environment: a case study of permian Lucaogou Formation, Jimusar sag. Xinjing Pet. Geol. 40 (3), 253–261 (in Chinese). https://doi.org/10.7657/XJPG20190301.
- Nelson, P.H., 2009. Pore-throat sizes in sandstones, tight sandstones, and shales. AAPG Bull. 93 (3), 329–340. https://doi.org/10.1306/10240808059.
- Olson, J., Laubach, S., Lander, R., 2009. Natural fracture characterization in tight gas sandstones: Integrating mechanics and diagenesis. AAPG Bull. 93 (11), 1535–1549. https://doi.org/10.1306/08110909100.
- Qiu, Z., Shi, Z., Dong, D., Lu, B., Zhang, C., Zhou, J., et al., 2016. Geological characteristics of source rock and reservoir of tight oil and its accumulation mechanism: a case study of Permian Lucaogou Formation in Jimusar sag, Junggar Basin. Petrol. Explor. Dev. 43 (6), 1013—1024. https://doi.org/10.1016/S1876-3804(16)30118-5.
- Qiu, Z., Zhao, W., Deng, S., 2012. Development prospect and strategic significance of tight gas and shale gas in China. Strategic Stud. CAE. 14 (6), 4–8+113 (in Chinese). https://doi.org/10.3969/j.issn.1009-1742.2012.06.001.
- Sibbit, A.M., Faivre, O., 1989. Dual lateral logging response of fractured rocks (translated by Lan-Qin Song). In: Proceedings of the 26th Annual Meeting of the Association of Well Logging Analysts. Petrol. Ind. Press, Beijing (in Chinese).
- Slatt, R.M., O'Brien, N.R., 2011. Pore types in the Barnett and Woodford gas shales: contribution to understanding gas storage and migration pathways in finegrained rocks. AAPG Bull. 95 (12), 2017–2030. https://doi.org/10.1306/ 03301110145.
- Tang, X., Jiang, Z., Jiang, S., Wang, P., Xiang, C., 2016. Effect of organic matter and maturity on pore size distribution and gas storage capacity in high-mature to post-mature shales. Energy & Fuels 30, 8985–8996. https://doi.org/10.1021/acs.energyfuels.6b01499.
- Tian, H., Pan, L., Xiao, X., Wilkins, R., Meng, Z., Huang, B., et al., 2013. A preliminary study on the pore characterization of Lower Silurian black shales in the Chuandong Thrust Fold Belt, southwestern China using low pressure N2 adsorption and FE-SEM methods. Mar. Petrol. Geol. 48, 8–19. https://doi.org/10.1016/j.marpetgeo.2013.07.008.
- Tian, W., Liu, H., He, S., Wang, J., Xie, L., et al., 2019. Characterization of microscopic pore structure of tight oil reservoirs in Lucaogou Formation, Jimusar Sag. Petrol. Geol. Recovery Effic. 26 (4), 24–32 (in Chinese). https://doi.org/10.13673/j.cnki.cn37-1359/te.2019.04.004.
- Thomas, R.D., Ward, D.C., 1972. Effect of overburden pressure and water saturation on gas permeability of tight sandstone cores. J. Petrol. Technol. 24 (2), 120–124. https://doi.org/10.2118/3634-PA.
- Wang, G., Sun, Z., Fu, J., Luo, X., Zhao, X., Pan, Y., 2015. Control factors and logging evaluation method for glutenite reservoir in Mabei area, Junggar Basin. Xinjing Pet. Geol. 36 (1), 8–13 (in Chinese). https://doi.org/10.7657/XJPG20150102.
- Wang, Y., Wang, H., Zhang, C., Li, X., Dong, D., 2017. Fracture pore evalution of the upper Ordovician wufeng to lower Silurian Longmaxi formations in southern Sichuan basin, SW China. Petrol. Explor. Dev. 44 (4), 531–539. https://doi.org/10.11698/PED.2017.04.06.
- Wu, L., Pang, X., Zhou, L., Pang, H., 2015. The quality evaluation and hydrocarbon generation and expulsion characteristics of Permian Lucaogou Formation

- source rocks in Jimusar sag, Junggar Basin. Acta Geol. Sin. 89, 283–286. https://doi.org/10.1111/1755-6724.12304.29
- Xu, H., Zhou, W., Zhang, R., Liu, S., Zhou, Q., 2019. Characterizations of pore, mineral and petrographic properties of marine shale using multiple techniques and their implications on gas storage capability for Sichuan Longmaxi gas shale field in China. Fuel 241, 360–371. https://doi.org/10.1016/j.fuel.2018.12.035.Yang, F., Ning, Z., Hu, C., Wang, B., Peng, K., Liu, H., 2013. Characterization of
- Yang, F., Ning, Z., Hu, C., Wang, B., Peng, K., Liu, H., 2013. Characterization of microscopic pore structures in shale reservoirs. Acta Petrol. Sin. 34 (2), 301–311 (in Chinese). https://doi.org/10.7623/syxb201302012.
- Yang, H., Chen, H., Bian, B., 2012. Structure modeling and geometry analysis in the western FuKang fault zone. Inner Mongolia petrochem. Ind. 38 (15), 138—140 (in Chinese).
- Zan, B., Liu, S., Bai, Z., Ran, B., Ye, Y., Qiu, J., et al., 2017. Pore characteristics of shale gas reservoir of Longmaxi Formation in Weiyuan Area, Southwest of Sichuan basin. Bull. Geol. Sci. Techol. 36 (2), 65–74 (in Chinese). https://doi.org/10.19509/j.cnki.dzka.2017.0208.
- Zeng, L., Ke, S., Liu, Y., 2010. Basic Theory and Methods of Low Permeability Oil and Gas Exploration. Petrol. Ind. Press, Beijing (in Chinese).
 Zhang, C., Zhu, Y., Chen, J., Li, Z., 2017. The comprehensive fractal characteristics of
- Zhang, C., Zhu, Y., Chen, J., Li, Z., 2017. The comprehensive fractal characteristics of shale and its influencing factors. J. Henan Polytech. Univ. (Natural Science). 36 (4), 42–47 (in Chinese). https://doi.org/10.16186/j.cnki.1673-9787.2017.04.007.
 Zhang, J., He, S., Yan, X., Hou, Y., Chen, X., 2017. Structural characteristics and
- Zhang, J., He, S., Yan, X., Hou, Y., Chen, X., 2017. Structural characteristics and thermal evolution of nanoporosity in shales. J. China Univ. Petrol. 41 (1) (in Chinese). https://doi.org/10.3969/i.issn.1673-5005.2017.01.002.
- Zhang, C., Zhu, D., Luo, Q., Liu, L., Liu, D., Yan, L., et al., 2017. Major factors controlling fracture development in the Middle Permian Lucaogou Formation tight oil reservoir, Junggar Basin, NW China. J. Asian Earth Sci. 146, 279—295. https://doi.org/10.1016/j.jseaes.2017.04.032.
- Zhang, C., Kong, X., Wang, Q., et al., 2025. Mechanisms of bedding fracturing in the Junggar Basin, northwest China: Constraints from in situ U-Pb dating and CO-Nd isotopic analysis of calcite cements. Geological Society of America Bulletin 137 (7–8), 3037–3054. https://doi.org/10.1130/B37973.1.
- Zhang, C., Liu, D., Jiang, Z., Song, Y., Luo, Q., Wang, X., 2022. Mechanism for the formation of natural fractures and their effects on shale oil accumulation in Junggar Basin, NW China. Int. J. Coal Geol. 254, 103973. https://doi.org/10.1016/ i.coal.2022.103973.
- Zhang, C., Wen, H., Wang, X., Wen, L., Shen, A., Zhou, G., Wang, Q., She, M., Ma, C., Qiao, Z., Liu, D., Ma, Y., 2024. Formational stages of natural fractures revealed by

- U-Pb dating and CO-Sr-Nd isotopes of dolomites in the Ediacaran Dengying Formation, Sichuan Basin, southwest China. GSA Bulletin 13 (11–12), 4671–4688. https://doi.org/10.1130/B37360.1.
- Zhang, C., Liu, D., Liu, Q., et al., 2023. Magmatism and hydrocarbon accumulation in sedimentary basins: A review. Earth-Science Reviews 244, 104531. https://doi.org/10.1016/j.earscirev.2023.104531.
- Zhang, X., Shi, W., Hu, Q., Zhai, G., Wang, R., Xu, F., et al., 2019. Pressure-dependent fracture permeability of marine shales in the Northeast Yunnan area, Southern China. Int. J. Coal Geol. 214, 103237. https://doi.org/10.1016/j.coal.2019.103237.
- Zhang, S., Liu, Y., Jiao, X., Zhou, D., Zhang, X., Lu, S., et al., 2018. Sedimentary environment and formation mechanism of dolomitic rocks in the middle Permian Lucaogou Formation, Jimusar Depression, Junggar Basin. J. Palaeogeogr. 20 (1), 33–48 (in Chinese). https://doi.org/10.7605/gdlxb.2018.01.003.
- Zhe, C., Liu, G., Kong, Y., Wang, C., Niu, Z., Zhang, J., et al., 2016. Lacustrine tight oil accumulation characteristics: permian Lucaogou Formation in Jimusaer sag, Junggar Basin. Int. J. Coal Geol. 153, 37–51. https://doi.org/10.1016/i.coal.2015.11.004.
- Zheng, X., Zhang, B., Sanei, H., Bao, H., Meng, Z., Wang, C., et al., 2019. Pore structure characteristics and its effect on shale gas adsorption and desorption behavior.
 Mar. Petrol. Geol. 100, 165–178. https://doi.org/10.1016/j.marpetgeo.2018.10.045.
- Zheng, M., Tian, A., Yang, T., He, W., Chen, L., Wu, H., et al., 2018. Structural evolution and hydrocarbon accumulation in the eastern Junggar Basin. Oil Gas Geol. 39 (5), 907–917. https://doi.org/10.11743/ogg20180506.
- Zhou, J., 2006. Characterization and Prediction of Fractured Buried Hill reservoirs. Petrol. Ind. Press, Beijing.
- Zou, C., Tao, S., Y, Z., Yuan, X., Zhu, R., Hou, L., et al., 2012. New advance in unconventional petroleum exploration and research in China. Bull. China Soc. Mineral Petrol. Geochem. 31 (4), 312–322 (in Chinese). https://doi.org/10.3969/j.issn. 1007-2802,2012.04.002.
- Zou, C., Zhai, G., Zhang, G., Wang, H., Zhang, G., Li, J., et al., 2015. Formation, distribution, potential and prediction of global conventional and unconventional hydrocarbon resources. Petrol. Explor. Dev. 42 (1), 13–25. https://doi.org/10.11698/PED.2015.01.02.
- Zou, C., Dong, D., Wang, S., Li, J., Li, X., Wang, Y., et al., 2010. Geological characteristics, formation mechanism and resource potential of shale gas in China. Petrol. Explor. Dev. 37 (6), 641–653. https://doi.org/10.1016/S1876-3804(11)60001-3.